

# A robust QRS detection and accurate R-peak identification algorithm for wearable ECG sensors

Kai ZHAO<sup>1</sup>, Yongfu LI<sup>1\*</sup>, Guoxing WANG<sup>1</sup>, Yu PU<sup>2</sup> & Yong LIAN<sup>1</sup>

<sup>1</sup>*Department of Micro and Nano Electronics, Shanghai Jiao Tong University, Shanghai 200240, China;*

<sup>2</sup>*Alibaba Group, Sunnyvale CA 94085, USA*

Received 9 August 2020/Revised 23 October 2020/Accepted 7 December 2020/Published online 8 May 2021

**Abstract** This paper presents a robust QRS detection algorithm that is capable of detecting QRS complexes as well as accurately identifying R-peaks. The proposed bilateral threshold scheme combined with QRS watchdog greatly improves the detection accuracy and robustness, resulting in consistent detection performance on 9 available ECG databases. Simulations show that the proposed algorithm achieves good results on the datasets from both QTDB healthy database and MITDB arrhythmia database, i.e. the sensitivity of 99.99% and 99.88%, the precision of 99.98% and 99.88%, and the detection error rate of 0.04% and 0.31%, respectively. Furthermore, it also outperforms many existing algorithms on six other ECG databases, such as NSTDB, TWADB, STDB, SVDB, AFTDB, and FANTASIADB.

**Keywords** signal processing, QRS detection, R-peak detection, wearable ECG sensors, bilateral threshold

**Citation** Zhao K, Li Y F, Wang G X, et al. A robust QRS detection and accurate R-peak identification algorithm for wearable ECG sensors. *Sci China Inf Sci*, 2021, 64(8): 182401, <https://doi.org/10.1007/s11432-020-3150-2>

## 1 Introduction

Electrocardiogram (ECG) is an electric potential signal generated by a large number of cardiomyocytes, measured by electrodes at specified positions on a human body. According to World Health Organization, cardiovascular diseases (CVDs) are the number 1 cause of death globally, representing 31% of all global deaths [1]. With the recent advancement in flexible electronics, low cost and easy to use wearable ECG sensors will be available in near future [2–9]. These wearable ECG sensors will change the landscape of managing CVD patients, saving millions of dollars in treating CVDs and in production loss.

As illustrated in Figure 1, ECG waveform is a quasi-periodic signal composed of repeating patterns, which can be marked by fiducial points, i.e., “P”, “Q”, “R”, “S”, and “T”. The “P” wave represents atrial depolarization, the “QRS” complex represents ventricular depolarization, and the “T” wave represents ventricular re-polarization [10]. The “QRS” complex has a distinct characteristic in ECG waveform, and its peak, also known as “R” peak, is the most important feature in ECG analysis. The segmentation between sequential “R” peaks is known as “R-R” interval.

“QRS” detection is an important step in ECG-related analytic applications, including heart rate (HR) monitoring [11], heart rate variability (HRV) analysis [10, 12–17], cardiac arrhythmia detection [18, 19], heartbeat classification [20–22], and identity recognition [23–26]. HRV can be used to detect early warning signs of congestive heart failure [27, 28] and obstructive sleep apnea [29, 30]. Thus, a “QRS” detection algorithm that is capable of accurately identifying R-peak location is highly sought.

ECG signals are normally contaminated by instrumental, muscle, and power-line noises. The first step in detecting “QRS” complexes is to reduce these noises. Existing “QRS” and R-peak detection algorithms [31–39] adopted signal level “threshold” technique(s) to determine the positions of “QRS” complexes and derived “R” peaks and “R-R” intervals. However, the detection accuracy is highly dependent on ECG morphology. Figure 2 shows 10 different types of ECG waveform from MITDB [40]. Most of “QRS” detection algorithms use MITDB to demonstrate their performance. Note that there are other

\* Corresponding author (email: [yongfu.li@sjtu.edu.cn](mailto:yongfu.li@sjtu.edu.cn))

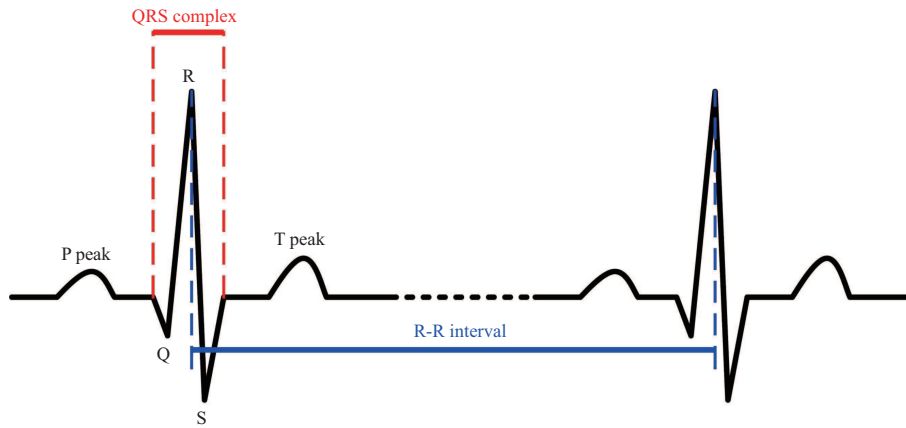


**Figure 1** (Color online) An example of ECG signal, marked with fiducial points “P”, “Q”, “R”, “S”, and “T”.

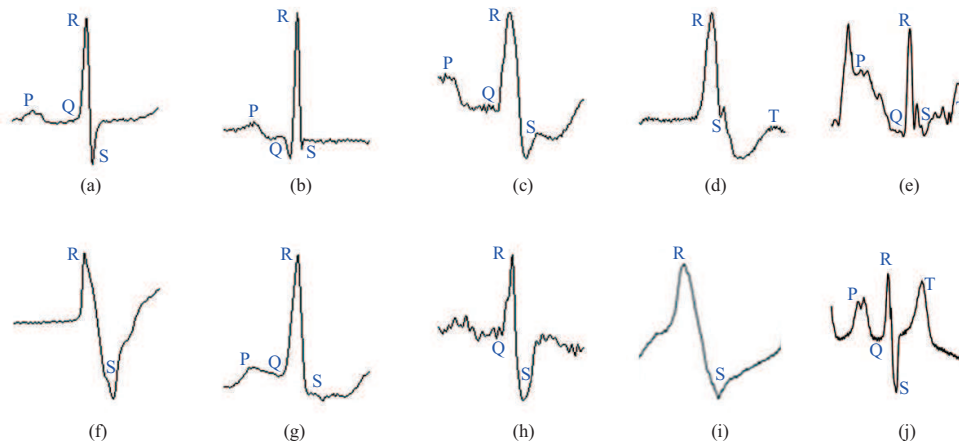


**Figure 2** (Color online) An example of ten different types of ECG beat from MITDB [40]. (a) Normal (NOR); (b) atrial premature contraction (APC); (c) left bundle branch block (LBB); (d) ventricular escape beat (VEB); (e) NOR with noise; (f) paced beat (PAB); (g) premature ventricular contraction (PVC); (h) right bundle branch block (RBB), (i) ventricular flutter wave (VFW); (j) aberrated atrial premature.

ECG databases such as QTDB [41], NSTDB [42], TWADB [43], STDB [44], SVDB [45], AFTDB [46], FANTASIADB [47], and INCARTDB [48]. A robust “QRS” detection algorithm should show good performance across different ECG databases. Such robustness may not be easily achieved. For example, the Pan and Tompkins [31] method has achieved the best performance on QTDB [41] (sensitivity (Se) of 99.54% and precision (+P) of 99.68%); however, its sensitivity on FANTASIADB has degraded to 82.70%. Note that the ECG signals recorded from the wearable flexible ECG sensors are very different from traditional resting ECG and Holter, i.e., the ECG morphology changes with the sensor location. So a robust “QRS” detection algorithm is highly thought of in dealing with the large variations in ECG morphology. This motivates us to develop a “QRS” detection algorithm that is able to maintain the detection accuracy across different databases.

In this paper, we present a robust “QRS” (R-QRS) detection algorithm that is optimized on MITDB and evaluated on eight other databases from PhysioNet without removing any record and segment, except for non-annotated beats. The rest of the paper is organized as follows. Section 2 describes the definitions of the nine PhysioNet databases [49] and the parameters used in the proposed algorithm. Section 3 provides details of the proposed algorithm. Section 4 describes evaluation criteria with experiment results. Finally, a conclusion is drawn in Section 5.

## 2 Preliminaries

There are a total of nine PhysioNet databases [40–49] being evaluated in our proposed R-QRS algorithm. These databases are collected from populations of different physical conditions, sampled at different frequencies and under different noise environments. A summary of each database is described as follows:

(1) **MITDB**. MIT-BIH Arrhythmia database [40] is collected from a population of arrhythmia patients, sampled at 360 Hz. It contains 48 records of 30 min. Lead II of this database is used for optimizing our parameters while the remaining databases are used for evaluation.

(2) **QTDB**. QT database [41] contains 105 records of 15 min, sampled at 250 Hz. We have excluded parts of the record without “R” peak annotations.

(3) **NSTDB**. MIT-BIH noise stress test database [42] includes 12 half-hour ECG records with different degrees of noise, sampled at 360 Hz. The records are created on two clean records from Lead II of the MIT-BIH arrhythmia database [40] with electromyography (EMG) artifact noise. The signal-to-noise ratios (SNRs) of these records range from  $-6$  to  $24$  dB.

(4) **TWADB**. T-wave alternans challenge database [43] contains 100 records from a population of cardiac patients and healthy controls, sampled at 500 Hz.

(5) **STDB**. MIT-BIH ST change database [44] includes 28 ECG recordings of varying lengths sampled at 360 Hz, most of which were recorded during exercise stress tests and which exhibit transient ST depression. In this database, the “QRS” complex labels in the segment from 395 to 518 ms in record 319 were missing, so we have deleted record 319 in our experiments.

(6) **SVDB**. MIT-BIH supraventricular arrhythmia database [45] includes 78 half-hour records of supraventricular arrhythmia patients, which complement with MIT-BIH Arrhythmia database and sampled at 128 Hz.

(7) **AFTDB**. AF termination challenge database [46] includes 80 one-minute records of atrial fibrillation (AF), sampled at 128 Hz.

(8) **FANTASIADB**. Fantasia database [47] contains 40 120-min records from healthy subjects, sampled at 250 Hz.

(9) **INCARTDB**. St Petersburg INCART 12-lead arrhythmia database [48] contains 75 30-min records from patients undergoing tests for coronary artery disease, sampled at 257 Hz. Lead I of this database is used in our experiments.

## 3 The proposed R-QRS algorithm

The flow chart of the proposed R-QRS algorithm is shown in Figure 3. It contains the proposed pre-processing method, “peak pre-selection (PPS)” procedure, “bilateral threshold” setting mechanism, and “QRS watchdog”. The pre-processing method aims to reduce noise and enhance “QRS” complex. The PPS algorithm identifies potential R-peak candidates, and the “bilateral threshold” determines R-peak from its candidates. The “QRS watchdog” recovers the missing “R” peaks using a search-back function. Each part of the proposed algorithm is discussed in Subsections 3.1 and 3.2.

### 3.1 The pre-processing

Pre-processing is commonly used to reduce noises and enhance “QRS” complexes in ECG signals. We noticed that existing methods [31, 32] are not very effective against noises as illustrated in Figure 4 while methods in [33–39, 50] are less sensitive to ventricular flutter beats. Thus, we proposed a new QRS enhancement technique that enhances the “QRS” complex while suppresses different types of noise. For a bandpass filtered ECG signal,  $y$ , the proposed QRS enhancement generates a QRS-enhanced signal,  $z$ , as follows:

$$z[n] = \frac{1}{2W+1} \sum_{k=0}^{2W} (y[n-W+k] - \hat{y}_n[k])^2, \quad (1)$$

where  $y$  is a band-pass filtered ECG signal. The cut-off frequencies  $f_1$  and  $f_2$  of the bandpass filter are optimized based on MITDB, whose values will be given in Subsection 4.2.  $W$  is the radius of a window centered at the time index  $n$ , and  $\hat{y}_n$  is defined as

$$\hat{y}_n[k] = \frac{k}{2W} (y[n+W] - y[n-W]) + y[n-W]. \quad (2)$$

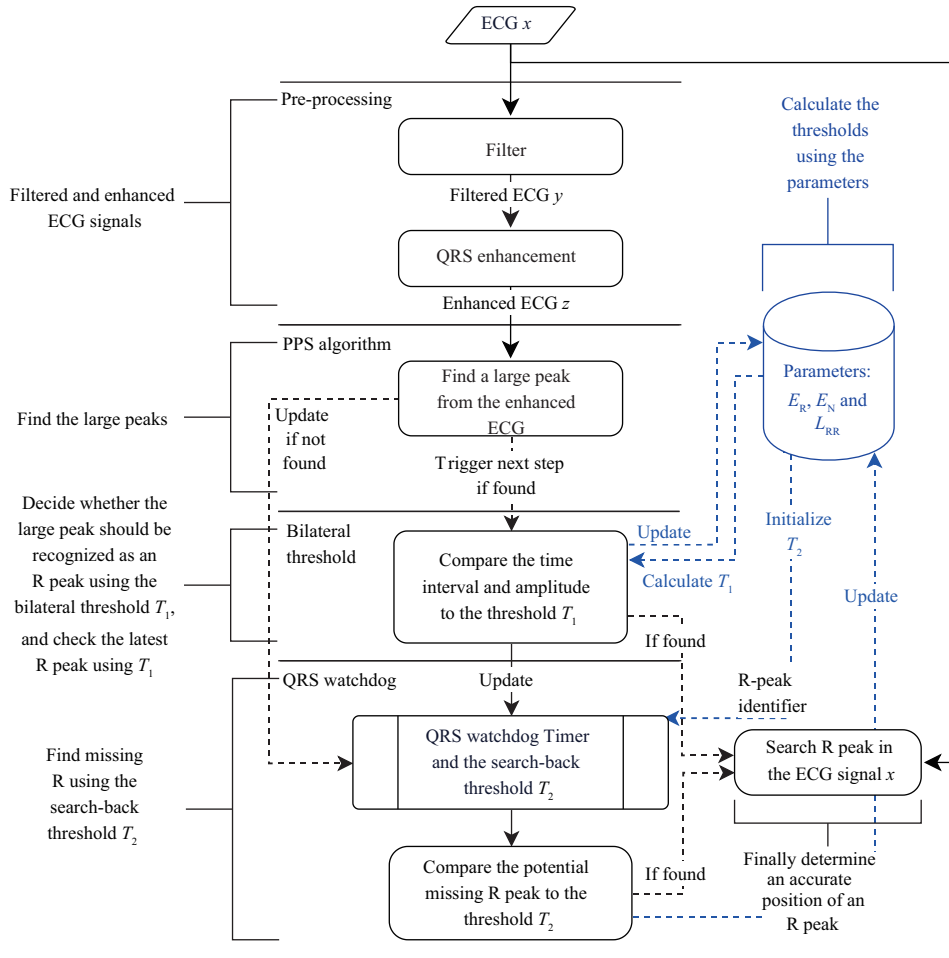


**Figure 3** (Color online) Flow chart of our proposed R-QRS algorithm.

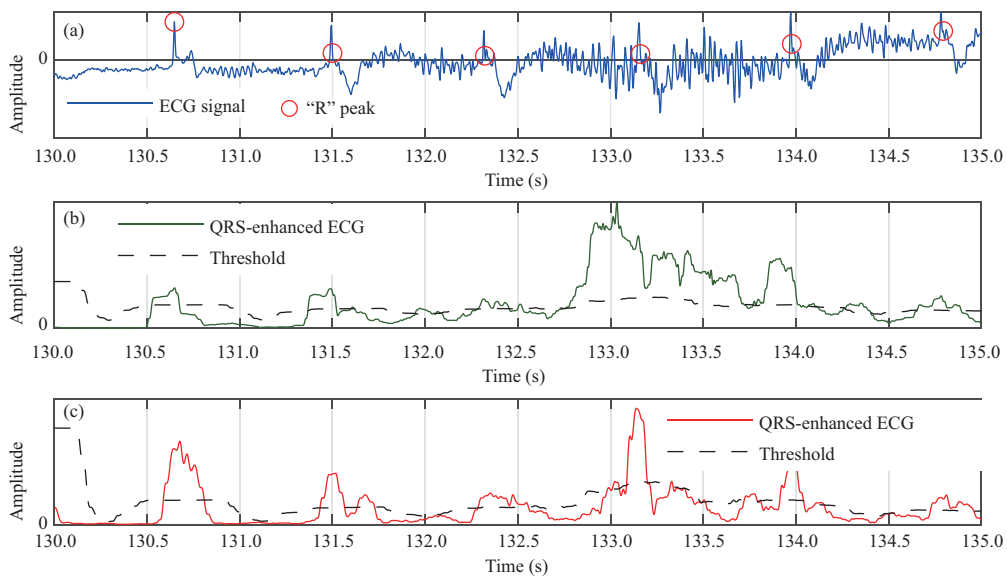


**Figure 4** (Color online) An example of (a) the ECG signal, (b) its enhanced “QRS” complexes after pre-processing [31], and (c) its enhanced “QRS” complexes after pre-processing [32].

If the window radius  $W$  is set properly (close to the duration of most “QRS” complexes), the proposed QRS enhancement is able to enhance the “QRS” complexes and reduce the interferences based on the

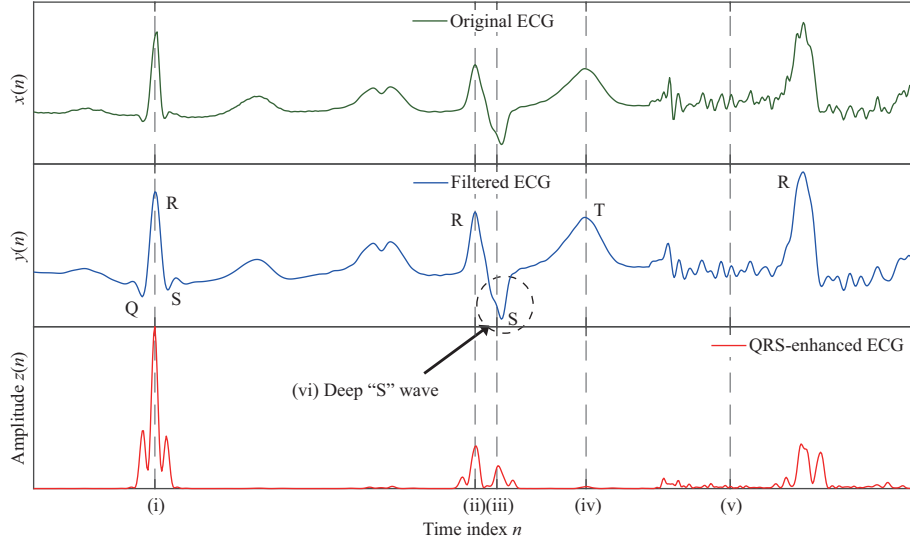


**Figure 5** (Color online) The relation among the original ECG, the filtered ECG, and the QRS-enhanced ECG.

following observations:

- (1) For a normal “QRS” complex,  $z[n]$  produces a local maximum at the “R” when the window  $[n - W, n + W]$  is centered at the “R” peak, as shown at location (i) in Figure 5.
- (2) In the case of an “R” followed by a deep “S” wave at locations (ii) and (iii) in Figure 5,  $z[n]$  produces two local maximums.
- (3) For an elevated “T” wave at location (iv) in Figure 5,  $z[n]$  becomes much smaller than that of an “R” peak. This is because a “T” wave is wider than that of the “QRS” complex.
- (4) For noises, their durations do not match the window width of  $2W + 1$ . So they will be suppressed as shown at location (v) in Figure 5.

Based on the above observations, the window width  $2W + 1$  should be wide enough to cover the duration of most “QRS” complexes, and it also should be as narrow as possible to avoid covering an elevated “T” wave. The value of  $W$  is optimized on MITDB, and the details can be found in Subsection 4.2.

Figure 6 provides different examples of the ECG signals and their corresponding QRS-enhanced ECG signals using the proposed technique. The proposed method is effective for different types of regular ECG, as shown in Figures 6(a) and (b). Clearly, the “R” peaks in Figures 6(a) and (b) can be detected using a simple constant threshold. However, there are still non-negligible “noise” peaks in the noisy ECG signals, as shown in Figures 6(c) and (d), and highly irregular “R” peaks in the arrhythmia ECG signal, as shown in Figure 6(e). Therefore, we propose the following “R” peak detection procedure for these complex scenarios.

### 3.2 The “R” peak detection procedure

The proposed “R” peak detection procedure detects potential “R” peaks in the QRS-enhanced ECG, and finds their exact locations of “R”. As illustrated in Figure 3, the “R” peak detection procedure consists of (1) “peak pre-selection” (PPS), (2) “bilateral threshold”, (3) “QRS watchdog”, and (4) “R-peak identifier” algorithms. For each pre-processed incoming ECG sample  $z[n]$ , the PPS algorithm finds a local maximum within a given time window. This peak is checked by the “bilateral threshold” algorithm to determine if it is an “R” peak or a “noise” peak. A search-back function, “QRS watchdog”, is used to pick up possible missing “R” peaks. Whenever an “R” peak is identified on  $z[n]$ , an actual “R” peak is marked on the corresponding raw ECG signal  $x[n]$  by the “R” peak identifier algorithm to complete the “R” peak detection process.

#### 3.2.1 The “peak pre-selection (PPS)” algorithm

The “peak pre-selection (PPS)” algorithm finds a local maximum  $A_0$  within a time window  $L_{\text{pre}} = 200$  ms.  $L_{\text{pre}}$  represents the shortest “R-R” interval in MITDB. To prevent large noise, such as motion artifacts, from distorting the “R” peak detection threshold,  $A_0$  is limited by an upper bound  $A_{\text{max}}$ ,

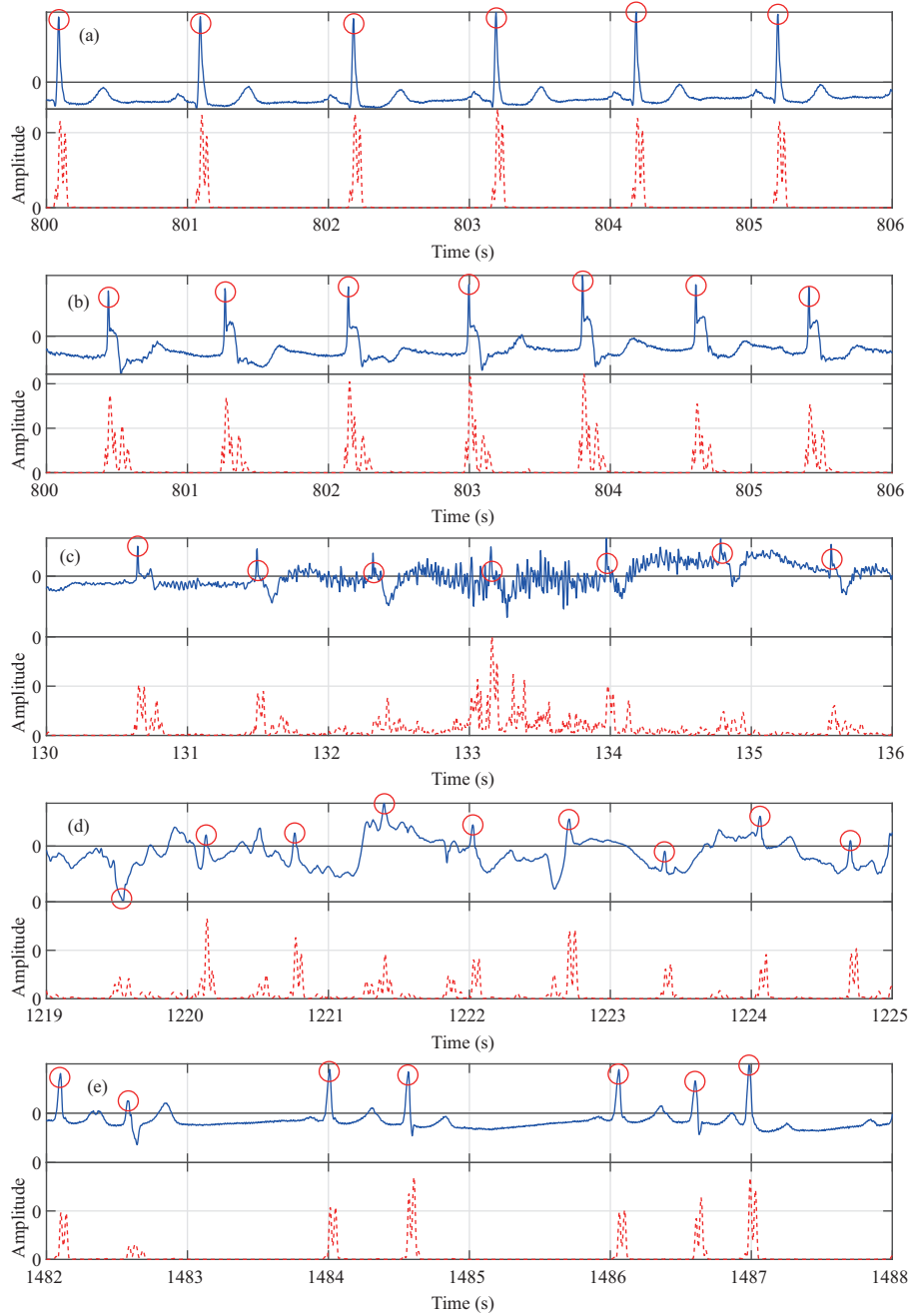


**Figure 6** (Color online) ECG signals (solid blue lines) and our QRS-enhanced ECG (dotted red line) from MITDB record (a) ‘101’, (b) ‘102’, (c) ‘104’, (d) ‘105’, and (e) ‘201’. The “R” peaks are denoted by red circles.

which is optimized based on MITDB. The local maximum  $A_0$  and its time index  $P_0$ , namely “large peak”, will be passed to the “bilateral threshold” algorithm (Subsection 3.2.2) to decide if this peak is considered as an “R” peak or “noise” peak.

### 3.2.2 The “bilateral threshold” algorithm

The “bilateral threshold” algorithm is performed on the detected large peak  $(P_0, A_0)$  from the PPS algorithm, to determine if this detected peak is considered as an “R” peak or “noise” peak. The algorithm uses an adaptive threshold  $T_1$  based on three predicted values, i.e., “R-R” interval  $L_{RR}$ , “R” peak  $E_R$ , and “noise” peak  $E_N$ . The predicted values are based on the most recent  $N_s$  numbers of “R-R” intervals  $L_i$ , “R” peaks  $A_i$ , and “noise” peaks  $B_i$ .

Note that not all the historical data are helpful in predicting  $L_{RR}$ ,  $E_R$  and  $E_N$ . For example, sudden

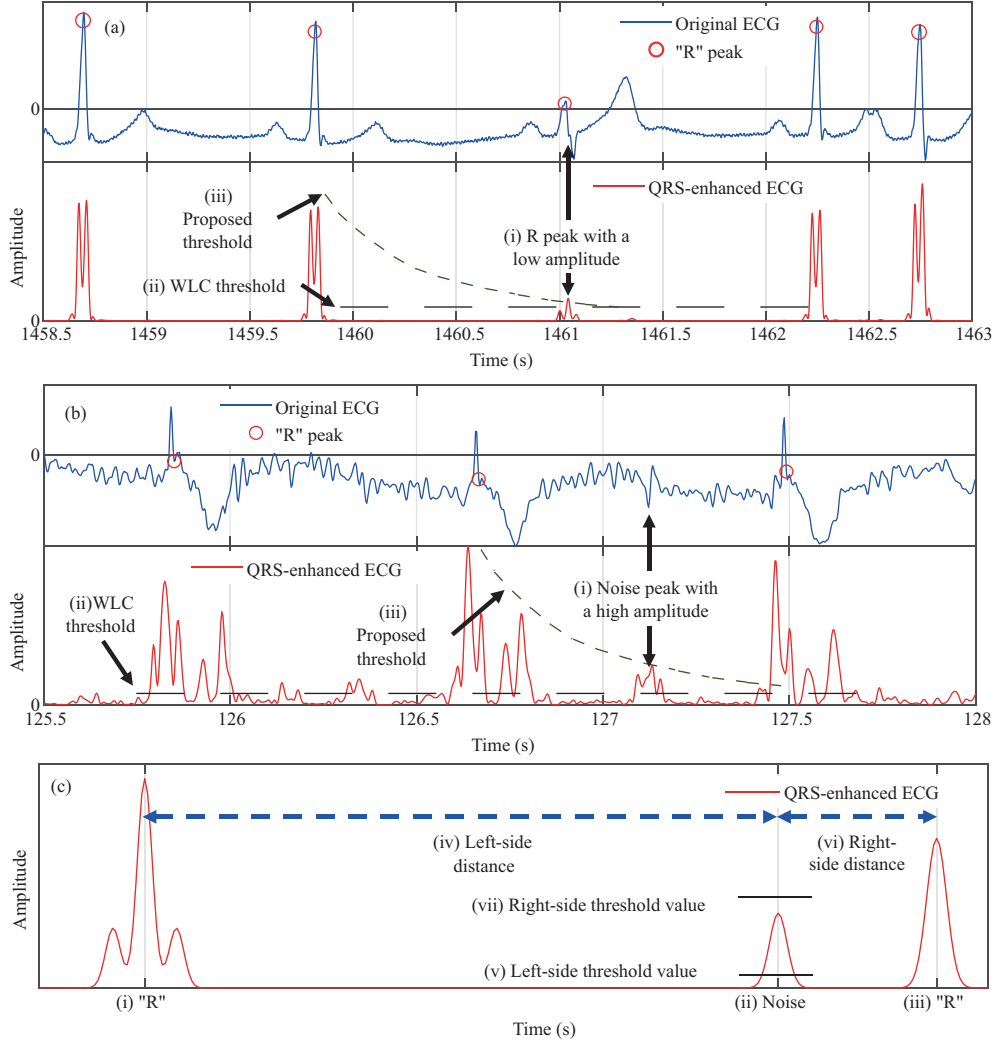


**Figure 7** (Color online) The different threshold setting strategies. (a) Record ‘205’ in MITDB; (b) record ‘104’ in MITDB; (c) bilateral threshold.

arrhythmia or large noise may cause extreme “R-R” intervals, “R” peak’s amplitudes, and “noise” peak’s amplitudes. These extreme values may distort the predicted values. To improve predictions, we first sort the stored  $L_i$ ,  $A_i$ , and  $B_i$  in ascending order. The predicted “R-R” interval is obtained by

$$L_{RR} = \frac{1}{N_s - 2N_e} \sum_{i=N_e+1}^{N_s-N_e} L_i, \quad (3)$$

where  $N_e$  is the number of discarded large and small values. The predicted “R” peak’s amplitude  $E_R$  and “noise” peak’s amplitude  $E_N$  are calculated by a similar method. The constant parameters  $N_s$  and  $N_e$  are being optimized on MITDB, and the details can be found in Subsection 4.2.

To determine whether a “large peak”,  $(P_0, A_0)$ , is an “R” peak or “noise” peak, the threshold,  $T_1$ , should be set between  $E_R$  and  $E_N$ . The weighted linear combination (WLC) of  $E_R$  and  $E_N$  is used in [31] to determine the threshold; however, such a strategy is not always effective. As shown in Figure 7(a), record ‘205’ in MITDB, to detect the “R” peak with a low amplitude at location (i), an extremely low constant threshold value must be set, which means the weight of  $E_N$  must be much larger than the weight of  $E_R$ . However, if the same set of weights is used for the threshold in record ‘104’ in MITDB, as shown in Figure 7(b), the large “noise” peak (i) will be wrongly marked as an “R” peak since its amplitude is higher than the threshold value. The problem can be solved by adopting an adaptive threshold setting strategy where the threshold value is dependent on the relative position between the R-peak candidate (“large peak”) and the latest detected “R” peak. For example, we regard the latest detected “R” peak before

the “large peak” as a “left-base point”, denoted by  $(P_{\text{last}}, A_{\text{last}})$ , and let the threshold value decrease as the interval  $|P_0 - P_{\text{last}}|$  increases (the tendencies of the threshold value are illustrated as dashed lines in Figure 7). Since the threshold value is dependent on the interval between the “large peak” and the “left-base point”, we denote it as  $T_1(P_0, P_{\text{last}})$  and call it “left-side threshold” afterward. Using the “left-side threshold”, the “R” peak at location (i) in Figure 7(a) will be detected since its amplitude exceeds the threshold value, and the “noise” peak at location (i) in Figure 7(b) will be excluded since its amplitude is lower than the threshold value. According to our preliminary experiments, by letting the threshold value exponentially decrease as the interval  $|P_0 - P_{\text{last}}|$  increases, the proposed algorithm can attain the highest accuracy in MITDB.

With the proposed “left-side threshold” setting strategy, there is still a possibility that a “noise” peak is wrongly detected as an “R” peak. As illustrated in Figure 7(c), the large peak (ii), which is located far away from the left-base point, can be wrongly detected as an “R” peak if the left-side threshold is used. To address the problem, we regard the “R” peak at location (iii) in Figure 7(c), which is on the right side of the peak (ii), as a “right-base point”, and propose a “right-side threshold” to double check the peak (ii). Similar to the “left-side threshold”, the value of the “right-side threshold” decreases exponentially from the distance of the “right-base point”. Let us denote the “right-base point” as  $(P_{\text{next}}, A_{\text{next}})$ , and the “right-side threshold” value as  $T_1(P_0, P_{\text{next}})$ . For each “large peak”,  $(P_0, A_0)$ , it is first checked by the “left-side threshold”,  $T_1(P_0, P_{\text{last}})$ . If the amplitude  $A_0$  exceeds  $T_1(P_0, P_{\text{last}})$ , the “large peak” will be regarded as a temporary “R” peak. When the next temporary “R” peak is detected, it will be regarded as the “right-base point” of  $(P_0, A_0)$ . The peak  $(P_0, A_0)$  will be checked against the right-side threshold  $T_1(P_0, P_{\text{next}})$ . If  $A_0$  is greater than the right-side threshold, it will be changed from a temporary “R” peak to an “R” peak.

We have observed that most of the “noise” peaks have extremely low amplitudes with occasional large amplitude “noise” peaks as illustrated in Figure 7(a). Hence, a lower bound of the threshold  $T_1$  is set between these peaks so that the “bilateral threshold” algorithm will exclude a large number of extremely low “noise” peaks and focus on a small number of high “noise” peaks. We denote such a lower bound as  $T_{1\text{low}}$  below.

The lower bound of the threshold  $T_1$  is set by

$$T_{1\text{low}} = E_N + K_0(E_R - E_N), \tag{4}$$

where  $K_0$  is a constant parameter used to optimize the level of  $T_{1\text{low}}$ . For a “large peak” positioned at  $P_0$  and a detected “R” peak positioned at  $P_c$  ( $P_c$  can be  $P_{\text{last}}$  or  $P_{\text{next}}$ ), a bilateral threshold, i.e.,  $T_1(P_0, P_{\text{last}})$  or  $T_1(P_0, P_{\text{next}})$ , is calculated using

$$T_1(P_0, P_c) = T_{1\text{low}} + K_1(E_R - T_{1\text{low}}) \cdot \exp\left(\frac{-|P_c - P_0|}{\sigma \cdot L_{\text{RR}}}\right), \tag{5}$$

where  $K_1$  and  $\sigma$  are two parameters used to optimize the threshold value  $T_1$ . To reduce the hardware resources, we have replaced the negative exponential function  $\exp(-\tau)$  in (5) with the following formula:

$$\exp(-\tau) \approx (1 + \tau + 0.5\tau^2)^{-1}, \tau \geq 0. \tag{6}$$

$K_1$  is a constant parameter, which is optimized on MITDB, and the details can be found in Subsection 4.2.

Since the noise level on the left and the right sides of an “R” peak can be different, we allow  $\sigma$  in (5) to take different values when calculating the left-side and right-side thresholds:

$$\sigma = \begin{cases} \sigma_l^{(1)}, & P_0 < P_c \text{ (left side threshold)}, \\ \sigma_r^{(1)}, & P_0 > P_c \text{ (right side threshold)}. \end{cases} \tag{7}$$

The parameters  $\sigma_l^{(1)}$  and  $\sigma_r^{(1)}$  are optimized on MITDB, and the details can be found in Subsection 4.2. As a result, the four constant parameters,  $K_0$ ,  $K_1$ ,  $\sigma_l^{(1)}$ , and  $\sigma_r^{(1)}$ , and the predicted values,  $L_{\text{RR}}$ ,  $E_R$ , and  $E_N$ , determine the value of the bilateral threshold,  $T_1$ . The decay rates of the “left-side threshold” and the “right-side threshold” are decided by the constant parameters  $\sigma_l^{(1)}$  and  $\sigma_r^{(1)}$ , respectively. According to (5), the upper bound of  $T_1$  is

$$T_{1\text{high}} = T_{1\text{low}} + K_1(E_R - T_{1\text{low}}). \tag{8}$$

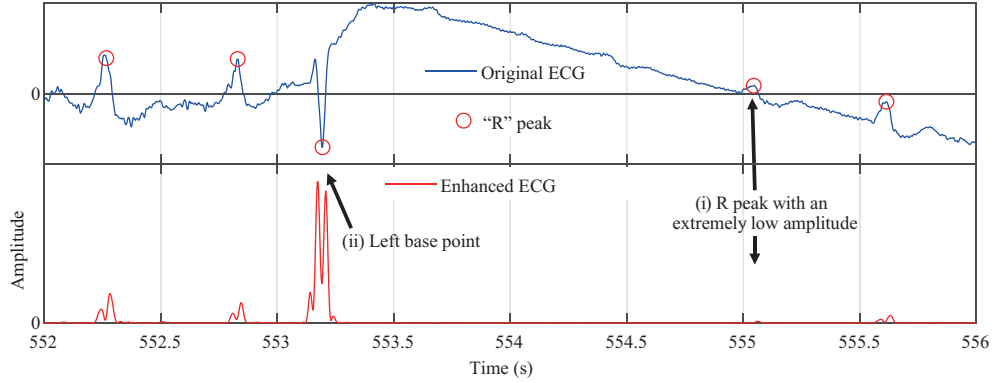


**Figure 8** (Color online) Record ‘203’ in MITDB.

Eqs. (8) and (4) show that the upper and lower bounds of  $T_1$  are decided by the constant parameters  $K_0$  and  $K_1$ .

### 3.2.3 The “QRS watchdog” algorithm

The “bilateral threshold” algorithm is effective in detecting “R” peaks, however, there might be scenarios causing missing “QRS” complexes. To improve the robustness of the “bilateral threshold” algorithm, we have also incorporated a “QRS watchdog” search-back function, where it tries to find out whether there is a missing “R” peak.

As illustrated in Figure 8, there is a 2.5-s cardiac arrest in the original ECG. When the heartbeat is restored at location (i) in Figure 8, its “R” peak has an extremely low amplitude. Since the previous “R” peaks have a larger amplitude, the value of the “left-side threshold” will be higher than the amplitude at location (i), which means the “R” peak cannot be detected by the “bilateral threshold” algorithm. Based on the above observations, the “QRS watchdog” algorithm is enabled when no “R” peak is detected during a long time-interval. Once the “QRS watchdog” algorithm is enabled, it initializes the search-back threshold  $T_2$  and quickly lowers threshold  $T_2$ , over time.

A counter  $\text{Timer}_R$  is used to track the time interval, which starts from zero and increases for each new sample. An upper bound  $L_{\text{miss}}$  is set for the counter as follows:

$$L_{\text{miss}} = K_{\text{miss}} \cdot L_{\text{RR}}, \quad (9)$$

where  $K_{\text{miss}}$  is a constant parameter used to optimize the upper bound  $L_{\text{miss}}$ . The algorithm tracks the highest “large peak” at  $(P_m, A_m)$  within the time interval  $(P_{\text{last}}, P_0]$ . When  $\text{Timer}_R$  exceeds  $L_{\text{miss}}$ , “QRS watchdog” algorithm is enabled. It begins to compare the amplitude  $A_m$  to the search-back threshold  $T_2$  at each new sample. If  $A_m$  exceeds  $T_2$ ,  $(P_m, A_m)$  is marked as an “R” peak on the QRS-enhanced ECG.

$\text{Timer}_R$  needs to be adjusted when a new “R” peak is determined. Specifically, it is reset to zero if an “R” peak is detected using the “left-side threshold”. It is set to  $P_0 - P_{\text{new}}$  if an “R” peak is detected by search-back threshold  $T_2$ , where  $P_0$  is the current time index. As a result, the count value of  $\text{Timer}_R$  always equals the time difference between the latest determined “R” peak and the current time index  $P_0$ . Whenever  $\text{Timer}_R$  is reset or a new “noise” peak is found by the “bilateral threshold algorithm”, the search-back threshold is reset to its initial value  $T_{1\text{low}}$ .

To detect the “R” peaks whose amplitudes are arbitrarily small, the search-back threshold  $T_2$  decreases at each new sample  $n$  using the following formula:

$$T_2[n] \leftarrow T_2[n-1] \cdot \exp\left(-\frac{1}{\sigma^{(2)} \cdot L_{\text{RR}}}\right), \quad (10)$$

where  $\sigma^{(2)}$  is a constant parameter used to optimize the decay rate of  $T_2$ . Again, the calculation of  $\exp(\cdot)$  can be simplified using (6). The function of this operation is similar to the “right-side threshold” in the “bilateral threshold” algorithm, i.e., ensuring that the highest peak, e.g., at location (iii) in Figure 7(c), can be found instead of the adjacent minor peaks, e.g., at location (ii) in Figure 7(c).

The constant parameters in this algorithm,  $K_{\text{miss}}$  and  $\sigma^{(2)}$ , are optimized on MITDB, and the details can be found in Subsection 4.2.

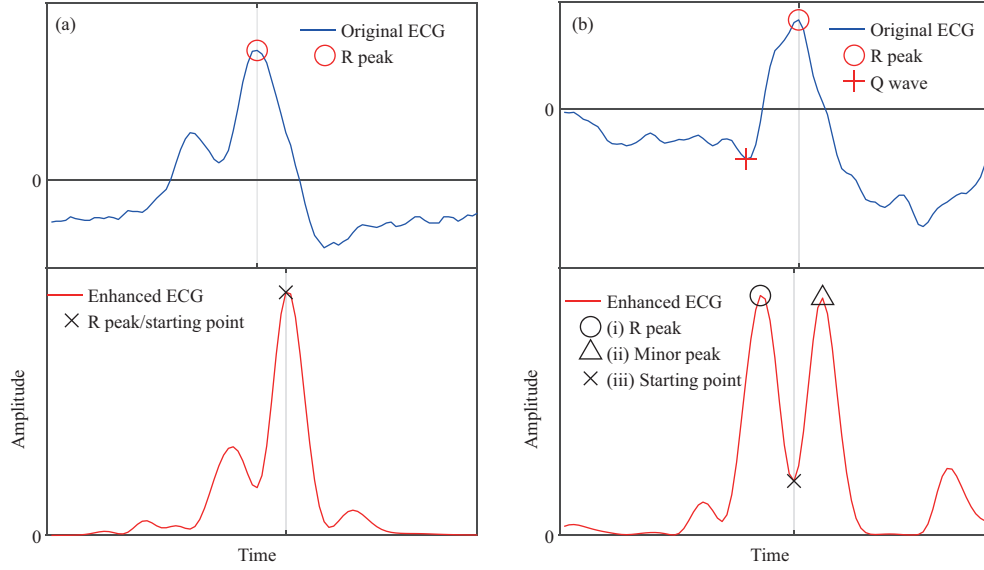


**Figure 9** (Color online) “R” peaks of different widths lead to different numbers of high peaks in the enhanced ECG. (a) A narrow “R” peak in the original ECG leads to a unique high peak in the enhanced ECG. (b) A wide “R” peak in the original ECG leads to two high peaks (the “R” peak and the minor peak) in the enhanced ECG.

### 3.2.4 The “R-peak identifier” algorithm

The algorithm presented so far is for “R” peak detection from the enhanced ECG signal. To accurately determine the “R” peak on the original ECG, the “R-peak identifier” algorithm first finds an approximate location based on the “R” peak on the enhanced ECG, denoted as the “starting point”, then it searches for the exact “R” peak location in the vicinity of the starting point.

Normally an “R” peak in the original ECG generates a unique high peak in the enhanced ECG signal, as illustrated in Figure 9(a). However, if the “QRS” complex on the original ECG is wider than the window used in the QRS enhancement (Subsection 3.1), the rising and falling edges of the original ECG will generate twin peaks on the enhanced ECG, which are illustrated in Figure 9(b) at locations (i) and (ii). In the case of Figure 9(b), if the detected “R” peak (i) is taken as the starting point, the location of “Q” wave might be wrongly identified as the exact location of “R” peak since it is much closer to the starting point than the true “R” peak. Hence, for an “R” peak on  $z[n]$  with time index and amplitude  $(P_0, A_0)$ , the “R peak identifier” algorithm searches for a second highest peak in a window  $[P_0 - 80, P_0 + 80]$  ms, denoted by  $(P_{\text{minor}}, A_{\text{minor}})$ . If  $A_{\text{minor}} > \frac{1}{2}A_0$ , the case of Figure 9(b) is considered, and the algorithm takes the midpoint between  $P_0$  and  $P_{\text{minor}}$  as the starting point. Otherwise,  $P_0$  is taken as the starting point.

Normally the starting point in the original ECG is on a slope, so that the top and bottom of the slope are taken as candidates for “R” peak. The direction of a “QRS” complex is usually upward in the leads, but sometimes it becomes bidirectional in MITDB [40]. A “sharpness score” (SC) is calculated to determine the likelihood of a candidate peak (the left or the right) is likely to be the accurate “R” peak:

$$SC(t_c, t_s) = \begin{cases} \left| \frac{x^{(2)}[t_c]}{t_s - t_c} \right|, & t_c - t_s \neq 0, \\ +\infty, & t_c - t_s = 0, \end{cases} \quad (11)$$

where  $t_s$  and  $t_c$  denote the time indexes of starting point and the candidate peak, respectively.  $x^{(2)}[t_c]$  denotes the second-order derivative of the ECG signal at time  $t_c$ , which is calculated by

$$x^{(2)}[t_c] = \frac{1}{2}x[t_c + 1] - x[t_c] + \frac{1}{2}x[t_c - 1]. \quad (12)$$

The candidate with the highest “SC” is determined as the accurate “R” peak. Since the second-order derivative characterizes the peak’s sharpness, this method tends to mark the sharpest peak as the “R” peak, as illustrated in Figure 10.

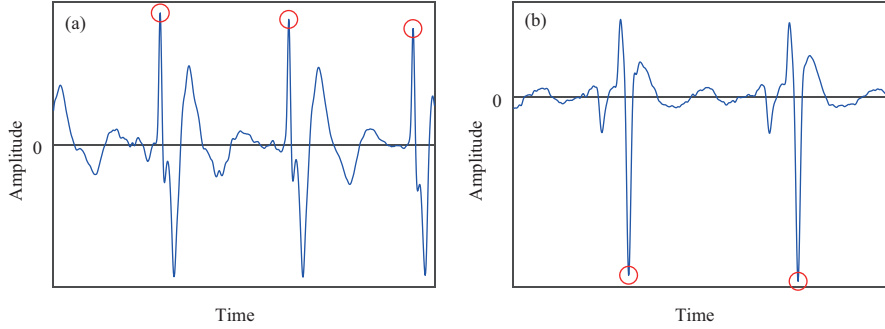


**Figure 10** (Color online) Examples of upward and downward “R” positions identified by the proposed “R-peak identifier” algorithm, denoted by red circles.

To achieve a more robust “R-peak identifier” algorithm, we only consider the points in a smaller window  $[t_s - F_l, t_s + F_r]$  that are marked as candidates, and if there is no candidate found in the window, the starting point is marked as an “R” peak. The parameters,  $F_l$  and  $F_r$ , are optimized in a range between 0 and 95 ms, which is the duration of normal “QRS” complexes [51]. The optimization is presented in Subsection 4.2.

In conclusion, the proposed “R” peak detection procedure can be written as the pseudo-code in Algorithm 1.

---

**Algorithm 1** Overall algorithm of dynamic “R” peak detection

---

**Require:**  $x, z$ . //The raw ECG signal and the QRS-enhanced ECG.

**Ensure:** The positions of the “R” peaks.

```

1: Parameters setup.
2: while New sample exists do
3:    $n \leftarrow n + 1$ ; //Increase time index.
4:    $(P_0, A_0) \leftarrow \text{PPS}(z, n)$ ; //Peak pre-selection.
5:   if  $P_0 \neq 0$  then
6:     // $P_0 \neq 0$  indicates that a “large peak” has been found.
7:     if  $A_0 > T_1(P_c, P_0)$  then
8:       Find an “R” on  $x$  by R-peak identifier;
9:       if the last “R” peak  $(P_c, A_c)$  was found by  $T_1$  rather than  $T_2$ , and  $A_c \leq T_1(P_0, P_c)$  then
10:        Treat  $(P_c, A_c)$  as an “noise” peak;
11:       end if
12:     else
13:       Take  $A_0$  as a “noise” peak;
14:     end if
15:     Update parameters;
16:   else
17:     //“Large peak” not found;
18:     Update QRS watchdog
19:     if QRS watchdog find a missing peak on  $z$  then
20:       Relocate missing “R” by QRS watchdog;
21:       Find an “R” on  $x$  by R-peak identifier;
22:     end if
23:   end if
24: end while
    
```

---

## 4 Experimental results and discussions

### 4.1 Evaluation criteria

Five evaluation criteria are adopted to evaluate the performance of the proposed R-QRS algorithm on 9 PhysioNet databases and compare their performances against the state-of-the-art algorithms [31–39].

By comparing the detected “QRS” complexes to the annotations of the databases, we obtain the number of correctly detected “QRS” complexes, TP; the number of wrong “R” labels given by the algorithm, FP; and the number of “QRS” complexes that are not detected by the algorithm, FN. Three common criteria (Definitions 1–3) are adopted based on TP, FP, and FN.

**Definition 1** (Sensitivity (Se)). The ratio between the number of correctly detected “QRS” complexes

TP to the total number of known “QRS” complexes [32]:

$$Se = \frac{TP}{TP + FN}. \quad (13)$$

**Definition 2** (Precision (+P)). The ratio between the number of correctly detected “QRS” complexes to the total number of detected “QRS” marks [32]:

$$+P = \frac{TP}{TP + FP}. \quad (14)$$

**Definition 3** (Detection error rate (DER)). The ratio between the total number of incorrectly “QRS” complexes to the total number of known “QRS” complexes [36]:

$$DER = \frac{FN + FP}{TP + FN}. \quad (15)$$

As Se, +P, and DER criteria are unable to provide a good measurement for the accuracy of “R” peak locations and “R-R” intervals, we have adopted a commonly-used time-domain method to measure HRV (Definition 4) and proposed two new criteria (Definitions 5 and 6).

**Definition 4** (Standard deviation of normal to normal (SDNN)). The standard deviation of the total number of identified “R-R” intervals (the distance between each heartbeat, or the “R” of the QRS complex) [12].

**Definition 5** (Error of HRV (EHRV)). We denote the number of records in a given database as  $N_{\text{sub}}$ . For each record in the database, there is an SDNN calculated using the “QRS” detection algorithm and an RSDNN (reference SDNN) calculated based on the annotated “QRS” information of the database. The  $N_{\text{sub}}$  SDNN and the  $N_{\text{sub}}$  RSDNN form two vectors respectively. EHRV is defined as the root mean square distance between the two vectors:

$$EHRV = \sqrt{\frac{1}{N_{\text{sub}}} \sum_{n=1}^{N_{\text{sub}}} (\text{SDNN}_n - \text{RSDNN}_n)^2}. \quad (16)$$

**Definition 6** (Annotated-detected error (ADE)). The root mean square time difference between the locations of the correctly detected “R” peak and the nearest annotated “R” peak:

$$\text{ADE} = \sqrt{\frac{1}{TP} \sum_{n=1}^{TP} (K_n - D_n)^2}. \quad (17)$$

In the  $n$ -th correctly detected “QRS” complex,  $K_n$  and  $D_n$  are the locations of “R” peaks annotated in the database and detected by the algorithm, respectively.

ADE is a non-negative value and it reaches zero if and only if the positions of all “R” peak locations in the correctly detected “QRS” complexes completely match the annotated peak locations.

## 4.2 Parameters optimization

In the proposed R-QRS algorithm, we have optimized all parameters based on the MITDB [40]. The optimized parameters are applied to the R-QRS algorithm to evaluate the performance of R-QRS on the remaining eight databases [41–48]. The optimization procedure aims at achieving the lowest DER. In total, there are 14 important parameters to be optimized, i.e.,  $f_1$ ,  $f_2$ ,  $W$ ,  $A_{\text{max}}$ ,  $N_s$ ,  $N_e$ ,  $K_0$ ,  $K_1$ ,  $K_{\text{miss}}$ ,  $\sigma_l^{(1)}$ ,  $\sigma_r^{(1)}$ ,  $F_l$ , and  $F_r$ , and we first initialize them empirically. Then, we set a step length for each parameter:  $\Delta f_1 = 1$  Hz,  $\Delta f_2 = 1$  Hz,  $\Delta W = 5$  ms,  $\Delta A_{\text{max}} = 0.05$  (mV)<sup>2</sup>,  $\Delta N_s = 1$ ,  $\Delta N_e = 1$ ,  $\Delta K_0 = 0.01$ ,  $\Delta K_1 = 0.01$ ,  $\Delta K_{\text{miss}} = 0.1$ ,  $\Delta \sigma_l^{(1)} = 0.01$ ,  $\Delta \sigma_r^{(1)} = 0.01$ ,  $\Delta \sigma^{(2)} = 0.01$ ,  $\Delta F_l = 10$  ms, and  $\Delta F_r = 10$  ms. In each iteration, we create 28 parameters by adding/subtracting a step length to/from each of them. The set of values that gives the lowest DER will be taken to the next iteration. Once the difference of DER between two successive iterations is lower than 0.01%, we take that set of values as the optimized ones. Finally, we have obtained the following values:  $f_1 = 3$  Hz,  $f_2 = 25$  Hz,  $W = 60$  ms,  $A_{\text{max}} = 1$  (mV)<sup>2</sup>,  $N_s = 10$ ,  $N_e = 1$ ,  $K_0 = 0.105$ ,  $K_1 = 1.250$ ,  $K_{\text{miss}} = 1.660$ ,  $\sigma_l^{(1)} = 0.18$ ,  $\sigma_r^{(1)} = 0.21$ ,  $\sigma^{(2)} = 0.73$ ,  $F_l = 80$  ms, and  $F_r = 60$  ms. We noticed that the optimization process is not sensitive to the initial values and the step lengths. Different initial values and step lengths lead to the same optimized parameters.

**Table 1** Evaluation of our “QRS” algorithm and state-of-the-art algorithms on nine open-source databases

Database	Method	Number of beats	Se (%)	+P (%)	DER (%)	EHRV (ms)	ADE (ms)
	<b>Our work</b>	<b>109966</b>	99.81	99.88	0.31	<b>44.6</b>	<b>12.2</b>
MITDB	Pan and Tompkins [31]	109966	99.13	99.63	1.24	$1.0 \times 10^4$	13.4
	Pandit et al. [37]	109809	99.65	99.66	–	–	–
	Elgendi et al. [32]	109966	99.71	99.85	0.44	77.2	32.3
	Chen et al. [39]	109494	99.89	<b>99.94</b>	–	–	–
	Lee et al. [33]	109481	99.69	99.88	–	–	–
	Martinez et al. [34]	109428	99.80	99.86	–	–	–
	Benitez et al. [35]	109456	99.13	99.31	–	–	–
	Modified Benitez et al. [35]	109456	99.29	99.24	–	–	–
	Hamilton and Tompkins [35]	109456	99.68	99.63	–	–	–
	Modified Hamilton-Tompkins [35]	109456	99.57	99.58	–	–	–
	Second derivative [35]	108228	98.08	99.18	–	–	–
Sahoo et al. [36]	44329	99.71	99.72	0.52	–	–	
	<b>Our work</b>	<b>86995</b>	<b>99.99</b>	<b>99.98</b>	<b>0.04</b>	<b>1.7</b>	<b>30.6</b>
QTDB	Pan and Tompkins [31]	86995	99.54	99.68	0.77	$7.4 \times 10^3$	31.3
	Pandit et al. [37]	86435	99.87	99.91	–	–	–
	Elgendi et al. [32]	86995	99.97	99.57	0.45	76.5	50.1
	Chen et al. [39]	114770	99.92	99.95	–	–	–
	Martinez et al. [34]	86892	99.92	99.88	–	–	–
	<b>Our work</b>	<b>25590</b>	<b>99.32</b>	<b>85.99</b>	<b>16.87</b>	<b>614.0</b>	<b>33.1</b>
NSTDB	Pan and Tompkins [31]	25590	96.34	85.85	19.53	$1.7 \times 10^5$	31.2
	Elgendi et al. [32]	25590	97.70	86.74	17.24	472.3	43.7
	<b>Our work</b>	<b>18991</b>	<b>99.18</b>	<b>98.37</b>	<b>2.52</b>	<b>402.5</b>	<b>32.2</b>
TWADB	Pan and Tompkins [31]	18991	96.94	98.21	4.83	$3.9 \times 10^4$	49.1
	Elgendi et al. [32]	18991	98.69	96.66	4.71	773.1	44.2
	<b>Our work</b>	<b>73616</b>	<b>99.93</b>	<b>99.83</b>	<b>0.19</b>	<b>2.2</b>	<b>15.1</b>
STDB	Pan and Tompkins [31]	73616	99.82	99.88	0.30	122.5	28.0
	Elgendi et al. [32]	73616	99.90	99.82	0.28	1.6	18.6
	<b>Our work</b>	<b>184583</b>	<b>99.93</b>	<b>99.87</b>	<b>0.20</b>	<b>5.0</b>	<b>21.9</b>
SVDB	Pan and Tompkins [31]	184583	99.82	99.88	0.30	10.4	29.3
	Elgendi et al. [32]	184583	99.56	99.49	0.95	5.4	45.0
	<b>Our work</b>	<b>7591</b>	<b>98.85</b>	<b>99.44</b>	<b>1.70</b>	<b>2.6</b>	<b>18.9</b>
AFTDB	Pan and Tompkins [31]	7591	98.99	99.27	1.74	4.0	21.3
	Elgendi et al. [32]	7591	98.56	99.23	2.20	4.5	30.5
	<b>Our work</b>	<b>285311</b>	<b>99.96</b>	<b>99.84</b>	<b>0.20</b>	<b>23.1</b>	<b>10.9</b>
FANTASIADB	Pan and Tompkins [31]	285311	82.70	99.86	17.42	$5.1 \times 10^8$	14.2
	Elgendi et al. [32]	285311	99.93	99.78	0.29	29.8	19.1
	<b>Our work</b>	<b>175906</b>	<b>98.72</b>	<b>95.52</b>	<b>5.92</b>	<b>169.5</b>	<b>21.0</b>
INCARTDB	Pan and Tompkins [31]	175906	94.45	96.10	9.37	$4.1 \times 10^6$	22.1
	Elgendi et al. [32]	175906	98.45	97.15	4.44	127.1	31.9

### 4.3 Experimental results

In this work, we have implemented two state-of-the-art “QRS” detection algorithms (Pan and Tompkins algorithm [31, 52] and Elgendi et al. algorithm [32] in MATLAB R2018b), along with their optimized parameters for a fair comparison. We did not implement algorithms that did not manage to identify all the beats in the MITDB [40]. These algorithms [33–36, 39] have excluded arrhythmia beats, resulting in a significant improvement in their Se and +P performance.

The benchmark results are listed in Table 1. The number of beats (the third column in Table 1) is the total number of beats being evaluated in each algorithm. It is worth noting that the number of beats used in our experiment in QTDB is not the same as in Chen et al. [39] because we have excluded the automatically determined ECG records according to the data description [41].

### 4.4 Discussions — performance on healthy subjects

For databases with healthy subjects, i.e., QTDB and FANTASIADB, the proposed R-QRS algorithm has achieved the best performance with the highest Se, +P, and the lowest DER compared to the state-of-the-art algorithms. Although our R-QRS algorithm is only optimized on the MITDB without

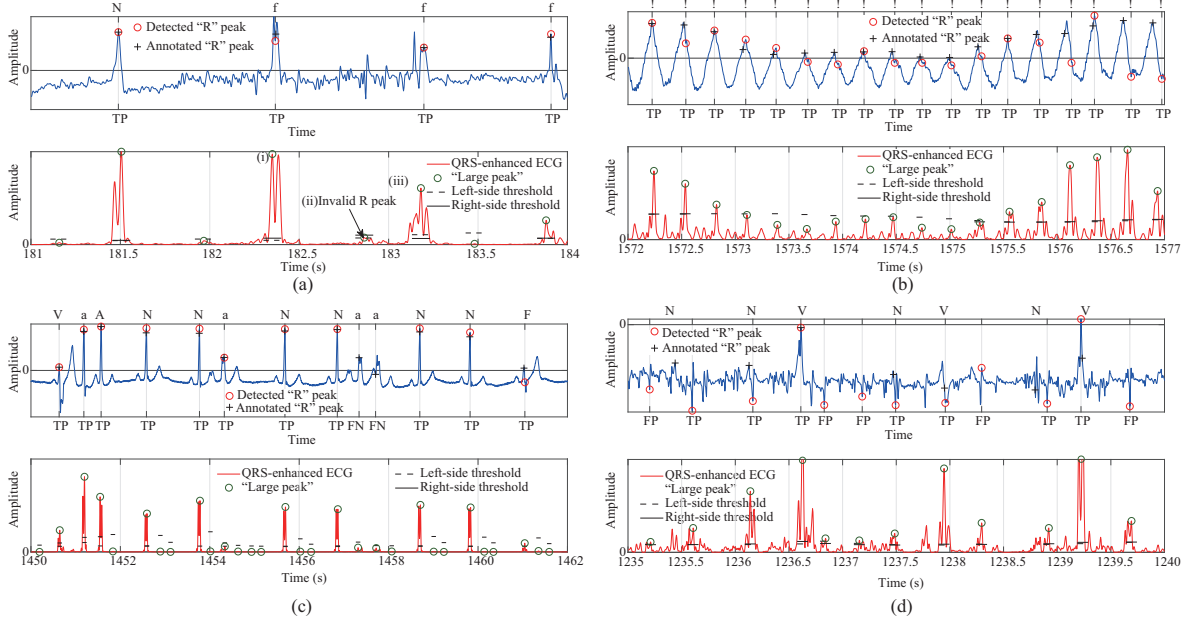


**Figure 11** (Color online) The representative original ECG signals (blue) and QRS-enhanced ECGs (red). The “R” peaks detected by R-QRS algorithm are marked by red circles. Record (a) ‘104’, (b) ‘207’, and (c) ‘201’ from MITDB; (d) record ‘I29’ from INCARTDB.

any exclusion of ECG records and ECG beats, we are still able to achieve very promising results with other databases [41–48]. On the contrary, Pan and Tompkins algorithm [31, 52] has missed a number of “QRS” complexes on TWADB and FANTASIADB databases because its dynamic threshold value does not decrease after a series of missing “QRS” complexes.

#### 4.5 Discussions — performance on SDNN and R-peak locations

Criteria EHRV and ADE are used to evaluate the accuracies of the R-peak locations. In particular, EHRV evaluates the accuracy in estimating the SDNN values, which is commonly used for evaluating HRV of normal ECG. Therefore, the result based on QTDB and FANTASIADB healthy databases will be the most important for our comparison on EHRV. As shown in Table 1, the proposed R-QRS algorithm achieves a smaller EHRV in six databases [40, 41, 43, 45–47] including the two healthy databases as compared to the state-of-the-art algorithms [31, 32]. Furthermore, our R-QRS algorithm has achieved the smallest ADE in eight out of nine databases [40, 41, 43–48]. There are very large EHRV values of Pan and Tompkins algorithm [31] in six databases [40–43, 47, 48], indicating that the SDNN strongly deviates from the RSDNN, because a number of successive “QRS” complexes are missed by its dynamic threshold and the search-back algorithms.

#### 4.6 Discussions — performance on arrhythmia ECG signals

For six out of seven arrhythmia databases [40, 42–46], our algorithm has achieved lower DER values compared to the algorithms [31, 32]. The good performance is the result of the “bilateral threshold” algorithm. We illustrate the advantages of “bilateral threshold” using several ECG segments from MITDB, as shown in Figure 11.

A representative segment of MITDB record ‘104’ is illustrated in Figure 11(a) to show how the bilateral threshold  $T_1$  helps to reduce the number of FNs and improve the robustness. “N” and “f” indicate the normal beat and the fusion of paced and normal beat, respectively. The large peak was first identified as an “R” peak because its amplitude exceeded the “left-side threshold”  $T_1$ . Once the immediate next “R” peak (marked as peak (iii) in Figure 11(a)) is detected, the “right-side threshold” is calculated based on the positions of peaks (ii) and (iii). Since the amplitude of peak (ii) is less than the “right-side threshold”, peak (ii) is declared as an invalid “R” peak.

We have observed that the ventricular flutter beats in MITDB record ‘207’ are hard to detect for the algorithms [31, 32]. In fact, we have obtained FN = 102 and FP = 6 using the algorithm [31], and obtained

**Table 2** Evaluation of the computational complexity of the proposed algorithm on MITDB

Method	Our work	Pan and Tompkins [31]	Elgendi et al. [32]
Computation time (s)	8.57	8.35	4.62

FN = 241 and FP = 6 using the algorithm [32]. It is also worth noting that the ventricular flutter beats in MITDB record ‘207’ have been excluded by Martinez et al. [34,39] from their experimental data. For the proposed algorithm, it achieves a more accurate result of FN = 26 and FP = 11 in comparison to [31,32] of FN = 102 and FP = 6. Although several “R” peaks’ amplitudes are lower than the left-side or right-side threshold, the “QRS watchdog algorithm” picks up them successfully. A representative segment of MITDB record ‘207’ is illustrated in Figure 11(b), where ‘!’ indicates ventricular flutter wave. Clearly, our algorithm has detected most of the beats in Figure 11(b) using the combination of the “bilateral threshold” and “QRS” watchdog algorithms.

We noticed that the proposed algorithm produces the highest FNs of 42 in record ‘201’ of MITDB. A representative segment of MITDB record ‘201’ is illustrated in Figure 11(c), where four types of heartbeats are marked. “N”, “V”, “A”, and “a” indicates NOR, PVC, APC, and aberrated atrial premature beats, respectively. All FNs are aberrated atrial premature beat. Our proposed “QRS watchdog” algorithm did not identify some of the missing “R” peaks in the aberrated atrial premature beat because the amplitudes of these peaks are too small and the signal has a varying rhythm.

We also noticed that the proposed algorithm attains a slightly higher DER than that of [32]. This is caused by record ‘I29’ in INCATDB, i.e., FN = 13 and FP = 690. The representative segment of ‘I29’ is shown in Figure 11(d). The large high frequency noises with comparable width to “R” peaks are enhanced by the QRS enhancement, leading to large FP. The algorithm [32] has achieved the lowest DER in INCARTDB because it tends to mark the uncertain peaks as “noise” peaks. Nevertheless, considering that the parameters of the proposed R-QRS are optimized on MITDB, its performance on most other databases is robust.

#### 4.7 Discussions — computational complexity

To evaluate the computational complexity of the proposed algorithm, we have tested the R-QRS algorithm and the two implemented algorithms [31,32] using MATLAB R2018b and an Intel Core i9-10900K processor at 5 GHz. The test was performed on MITDB to cover most types of ECG. The time taken to process all the records in MITDB are listed in Table 2. The R-QRS algorithm takes slightly longer time than the algorithms [31,32] with enhanced performance across different databases. The extra time is due to the use of the proposed “QRS enhancement” method and “R-peak identifier” to improve the accuracy of “R” peaks.

## 5 Conclusion

We have presented an R-QRS algorithm, with the combined use of “peak pre-selection”, “bilateral threshold”, and “R-peak identifier” algorithms, to detect the locations of “QRS” complexes and “R” peaks. For a more robust detection under varying ECG signal condition, we have also incorporated the “QRS watchdog” algorithm. We also proposed two criteria, ADE and EHRV, to evaluate the performance of detected “R” peak locations, which has an impact to HRV accuracy. By optimizing the parameters of the proposed R-QRS algorithm on MITDB and evaluating it on the remaining eight PhysioNet databases, the proposed R-QRS algorithm achieves  $Se = 99.99\%$ ,  $+P = 99.98\%$ , and  $DER = 0.04\%$  on the healthy database, QTDB, and it achieves  $Se = 99.81\%$ ,  $+P = 99.88\%$ , and  $DER = 0.31\%$  on arrhythmia database, MITDB. For the rest of the databases, the proposed algorithm has shown better or comparable performance, which highlights the robustness of the algorithm.

**Acknowledgements** This work was supported in part by National Key Research and Development Program of China (Grant No. 2019YFB2204500), in part by National Natural Science Foundation of China (Grant No. 61874171), in part by Science, Technology and Innovation Action Plan of Shanghai Municipality, China (Grant No. 1914220370), and Alibaba Group through Alibaba Innovative Research (AIR) Program.

#### References

- 1 World Health Organization. Cardiovascular diseases (CVDs). 2020. [https://www.who.int/news-room/fact-sheets/detail/cardiovascular-diseases-\(cvds\)](https://www.who.int/news-room/fact-sheets/detail/cardiovascular-diseases-(cvds))

- 2 Ravanshad N, Rezaee-Dehsorkh H, Lotfi R, et al. A level-crossing based QRS-detection algorithm for wearable ECG sensors. *IEEE J Biomed Health Inf*, 2014, 18: 183–192
- 3 Wong D L T, Yu J F, Li Y F, et al. An integrated wearable wireless vital signs biosensor for continuous inpatient monitoring. *IEEE Sensors J*, 2020, 20: 448–462
- 4 Luo Y X, Teng K H, Li Y F, et al. A 74- $\mu$ W 11-Mbps wireless vital signs monitoring SoC for 3-Lead ECG, respiration rate, and body temperature. *IEEE Trans Biomed Circ Syst*, 2019, 13: 907–917
- 5 Zhang X Y, Zhang Z, Li Y F, et al. A 2.89  $\mu$ W dry-electrode enabled clockless wireless ECG SoC for wearable applications. *IEEE J Solid-State Circ*, 2016, 51: 2287–2298
- 6 Zhang Q R, Xie Q S, Duan K F, et al. A digital signal processor (DSP)-based system for embedded continuous-time cuffless blood pressure monitoring using single-channel PPG signal. *Sci China Inf Sci*, 2020, 63: 149402
- 7 Dong X, Zhang M X, Lei Y H, et al. Parylene-MEMS technique-based flexible electronics. *Sci China Inf Sci*, 2018, 61: 060419
- 8 Zou X D, Xu X Y, Tan J, et al. A 1-v 1.1- $\mu$ w sensor interface ic for wearable biomedical devices. In: *Proceedings of IEEE International Symposium on Circuits and Systems*, 2008. 2725–2728
- 9 Liu L T, Liu Y, Duan X F. Graphene-based vertical thin film transistors. *Sci China Inf Sci*, 2020, 63: 201401
- 10 Khan M G. *Rapid ECG Interpretation*. Berlin: Springer, 2008
- 11 Xie Q S, Li Y F, Wang G X, et al. An unobtrusive system for heart rate monitoring based on ballistocardiogram using Hilbert transform and Viterbi decoding. *IEEE J Emerg Sel Top Circ Syst*, 2019, 9: 635–644
- 12 Xhyheri B, Manfrini O, Mazzolini M, et al. Heart rate variability today. *Prog Cardiovasc Dis*, 2012, 55: 321–331
- 13 Zhang F, Lian Y. Novel QRS detection by CWT for ECG sensor. In: *Proceedings of IEEE Biomedical Circuits and Systems Conference*, 2007. 211–214
- 14 Zhang F, Lian Y. Electrocardiogram QRS detection using multiscale filtering based on mathematical morphology. In: *Proceedings of the 29th Annual International Conference of the IEEE Engineering in Medicine and Biology Society*, 2007. 3196–3199
- 15 Zhang F, Tan J, Lian Y. An effective QRS detection algorithm for wearable ECG in body area network. In: *Proceedings of IEEE Biomedical Circuits and Systems Conference*, 2007. 195–198
- 16 Zhang F, Lian Y. QRS detection based on multiscale mathematical morphology for wearable ECG devices in body area networks. *IEEE Trans Biomed Circ Syst*, 2009, 3: 220–228
- 17 Zhang F, Lian Y. QRS detection based on morphological filter and energy envelope for applications in body sensor networks. *J Sign Process Syst*, 2011, 64: 187–194
- 18 Thong T, McNames J, Aboy M, et al. Prediction of paroxysmal atrial fibrillation by analysis of atrial premature complexes. *IEEE Trans Biomed Eng*, 2004, 51: 561–569
- 19 Jun T J, Park H J, Minh N H, et al. Premature ventricular contraction beat detection with deep neural networks. In: *Proceedings of the 15th IEEE International Conference on Machine Learning and Applications (ICMLA)*, 2016. 859–864
- 20 de Chazal P, O'Dwyer M, Reilly R B. Automatic classification of heartbeats using ECG morphology and heartbeat interval features. *IEEE Trans Biomed Eng*, 2004, 51: 1196–1206
- 21 Ye C, Kumar B V K V, Coimbra M T. Heartbeat classification using morphological and dynamic features of ECG signals. *IEEE Trans Biomed Eng*, 2012, 59: 2930–2941
- 22 Llamedo M, Martínez J P. Heartbeat classification using feature selection driven by database generalization criteria. *IEEE Trans Biomed Eng*, 2011, 58: 616–625
- 23 Wang J, She M, Nahavandi S, et al. Human identification from ECG signals via sparse representation of local segments. *IEEE Signal Process Lett*, 2013, 20: 937–940
- 24 He C G, Li W, Chik D. Waveform compensation of ECG data using segment fitting functions for individual identification. In: *Proceedings of the 13th International Conference on Computational Intelligence and Security (CIS)*, 2017. 475–479
- 25 Safie S I, Soraghan J J, Petropoulakis L. ECG biometric authentication using pulse active width (PAW). In: *Proceedings of IEEE Workshop on Biometric Measurements and Systems for Security and Medical Applications (BIOMS)*, 2011
- 26 Kaveh A, Chung W. Temporal and spectral features of single lead ECG for human identification. In: *Proceedings of IEEE Workshop on Biometric Measurements and Systems for Security and Medical Applications (BIOMS)*, 2013. 17–21
- 27 Yu S N, Lee M Y. Bispectral analysis and genetic algorithm for congestive heart failure recognition based on heart rate variability. *Comput Biol Med*, 2012, 42: 816–825
- 28 Yu S N, Lee M Y. Conditional mutual information-based feature selection for congestive heart failure recognition using heart rate variability. *Comput Meth Prog Biom*, 2012, 108: 299–309
- 29 Babaeizadeh S, White D P, Pittman S D, et al. Automatic detection and quantification of sleep apnea using heart rate variability. *J Electrocardiology*, 2010, 43: 535–541
- 30 Yildiz A, Akin M, Poyraz M. An expert system for automated recognition of patients with obstructive sleep apnea using electrocardiogram recordings. *Expert Syst Appl*, 2011, 38: 12880–12890
- 31 Pan J, Tompkins W J. A real-time QRS detection algorithm. *IEEE Trans Biom Eng*, 1985, 32: 230–236
- 32 Elgendi M. Fast QRS detection with an optimized knowledge-based method: evaluation on 11 standard ECG databases. *PLoS ONE*, 2013, 8: 73557
- 33 Lee J, Jeong K, Yoon J, et al. A simple real-time QRS detection algorithm. In: *Proceedings of the 18th Annual International Conference of IEEE Engineering in Medicine and Biology Society*, 1996. 1396–1398
- 34 Martínez J P, Almeida R, Olmos S, et al. A wavelet-based ECG delineator: evaluation on standard databases. *IEEE Trans Biomed Eng*, 2004, 51: 570–581
- 35 Arzeno N M, Deng Z D, Poon C S. Analysis of first-derivative based QRS detection algorithms. *IEEE Trans Biomed Eng*, 2008, 55: 478–484
- 36 Sahoo S, Biswal P, Das T, et al. De-noising of ECG signal and QRS detection using Hilbert transform and adaptive thresholding. *Procedia Tech*, 2016, 25: 68–75
- 37 Pandit D, Zhang L, Liu C Y, et al. A lightweight QRS detector for single lead ECG signals using a max-min difference algorithm. *Comput Meth Prog Biom*, 2017, 144: 61–75
- 38 Wang S K, Pang B, Liu M, et al. A novel compression framework using energy-sensitive QRS complex detection method for a mobile ECG. *Sci China Inf Sci*, 2019, 62: 069409
- 39 Chen H J, Maharatna K. An automatic R and T peak detection method based on the combination of hierarchical clustering and discrete wavelet transform. *IEEE J Biom Health Inform*, 2020, 24: 2825–2832
- 40 Moody G B, Mark R G. The impact of the MIT-BIH arrhythmia database. *IEEE Eng Med Biol Mag*, 2001, 20: 45–50
- 41 Laguna P, Mark R G, Goldberger A, et al. A database for evaluation of algorithms for measurement of QT and other waveform

- intervals in the ECG. In: Proceedings of Computers in Cardiology, 1997. 673–676
- 42 Moody G B, Muldrow W, Mark R G. A noise stress test for arrhythmia detectors. *Comput Cardiology*, 1984, 11: 381–384
- 43 Moody G. The physionet/computers in cardiology challenge 2008: T-wave alternans. In: Proceedings of Computers in Cardiology, 2008. 505–508
- 44 Albrecht P. ST segment characterization for long term automated ECG analysis. Dissertation for Ph.D. Degree. Cambridge: Massachusetts Institute of Technology, 1983
- 45 Greenwald S D, Patil R S, Mark R G. Improved detection and classification of arrhythmias in noise-corrupted electrocardiograms using contextual information. In: Proceedings of Computers in Cardiology, 1990. 461–464
- 46 Moody G. Spontaneous termination of atrial fibrillation: a challenge from Physionet and computers in cardiology 2004. In: Proceedings of Computers in Cardiology, 2004. 101–104
- 47 Iyengar N, Peng C K, Morin R, et al. Age-related alterations in the fractal scaling of cardiac interbeat interval dynamics. *Am J Phys-Regul Integr Comp Phys*, 1996, 271: 1078–1084
- 48 Mann D L, Zipes D P, Libby P, et al. Braunwald's Heart Disease E-Book: A Textbook of Cardiovascular Medicine. Amsterdam: Elsevier Health Sciences, 2014
- 49 Goldberger A L, Amaral L A N, Glass L, et al. PhysioBank, PhysioToolkit, and PhysioNet: components of a new research resource for complex physiologic signals. *Circulation*, 2000, 101: 215–220
- 50 Lian Y, Yu J H. The reduction of noises in ECG signal using a frequency response masking based fir filter. In: Proceedings of IEEE International Workshop on Biomedical Circuits and Systems, 2004
- 51 de Luna A B, Batchvarov V N, Malik M. The morphology of the electrocardiogram. In: The ESC Textbook of Cardiovascular Medicine. Oxford: Blackwell Publishing, 2006
- 52 Sedghamiz H. Matlab implementation of Pan Tompkins ECG QRS detector. Mathworks, 2014. <https://www.mathworks.com/matlabcentral/fileexchange/45840-complete-pan-tompkins-implementation-ecg-qrs-detector>